All-near-infrared multiphoton microscopy interrogates intact tissues at deeper imaging depths than conventional single- and two-photon near-infrared excitation microscopes

Pinaki Sarder
Siavash Yazdanfar
Walter J. Akers
Rui Tang
Gail P. Sudlow
Christopher Egbulefu
Samuel Achilefu

All-near-infrared multiphoton microscopy interrogates intact tissues at deeper imaging depths than conventional single- and two-photon near-infrared excitation microscopes

Pinaki Sarder,[a*] **Siavash Yazdanfar,**[b*] **Walter J. Akers,**[a] **Rui Tang,**[a] **Gail P. Sudlow,**[a] **Christopher Egbulefu,**[a] **and Samuel Achilefu**[a,c,d]

[a]Washington University, Department of Radiology, 4225 Scott Avenue, St. Louis, Missouri 63108
[b]GE Global Research, Applied Optics Lab, 1 Research Circle, Niskayuna, New York 12309
[c]Washington University, Department of Biomedical Engineering, 4225 Scott Avenue, St. Louis, Missouri 63108
[d]Washington University, Department of Biochemistry & Molecular Biophysics, 4225 Scott Avenue, St. Louis, Missouri 63108

Abstract. The era of molecular medicine has ushered in the development of microscopic methods that can report molecular processes in thick tissues with high spatial resolution. A commonality in deep-tissue microscopy is the use of near-infrared (NIR) lasers with single- or multiphoton excitations. However, the relationship between different NIR excitation microscopic techniques and the imaging depths in tissue has not been established. We compared such depth limits for three NIR excitation techniques: NIR single-photon confocal microscopy (NIR SPCM), NIR multiphoton excitation with visible detection (NIR/VIS MPM), and all-NIR multiphoton excitation with NIR detection (NIR/NIR MPM). Homologous cyanine dyes provided the fluorescence. Intact kidneys were harvested after administration of kidney-clearing cyanine dyes in mice. NIR SPCM and NIR/VIS MPM achieved similar maximum imaging depth of ~100 μm. The NIR/NIR MPM enabled greater than fivefold imaging depth (>500 μm) using the harvested kidneys. Although the NIR/NIR MPM used 1550-nm excitation where water absorption is relatively high, cell viability and histology studies demonstrate that the laser did not induce photothermal damage at the low laser powers used for the kidney imaging. This study provides guidance on the imaging depth capabilities of NIR excitation-based microscopic techniques and reveals the potential to multiplex information using these platforms. © *The Authors. Published by SPIE under a Creative Commons Attribution 3.0 Unported License. Distribution or reproduction of this work in whole or in part requires full attribution of the original publication, including its DOI.* [DOI: 10.1117/1.JBO.18.10.106012]

1 Introduction

Fluorescence microscopy has set the standard for structural resolution and molecular detection in biological tissues. Unfortunately, fluorescence detection is limited in depth by wavelength-dependent attenuation of light in such tissues. By improving the focus of excitation and significantly reducing background signal, recent advances in nonlinear optics have enabled higher imaging depth through multiphoton excitation. Microscopy of thick tissue sections (>0.5 mm) and living animals requires greater imaging depth relative to cells. Although optical imaging methods are limited in depth profiling versus other clinical imaging modalities such as nuclear, computed tomography, and magnetic resonance imaging, intravital microscopy enables unparalleled spatial resolution, offering the potential of noninvasive histology for interrogating superficial regions.[1] As a result, it can provide real-time assessment of suspicious tissues and surgical margins without resorting to traditional *ex vivo* histologic analysis.

The high autofluorescence and light scattering in the visible wavelengths provide adequate contrast for imaging cells and tissues. However, these optical features produce undesirable background signal in molecular imaging microscopy with exogenous fluorescent probes. This condition becomes severe at the usual low concentrations of targeted fluorescent probes in biological systems, requiring strategies that reduce autofluorescence and improve the signal-to-noise ratio. Researchers have addressed these issues by performing fluorescence imaging at near-infrared (NIR) wavelengths to minimize autofluorescence and increase imaging depth.[2] Diverse NIR fluorescent molecular probes have been developed as alternatives to traditional visible fluorophores for imaging molecular processes across spatial scales ranging from cells and tissues to living organisms.

The emergence of multiphoton microscopy (MPM) has sparked the advancement of deep-tissue fluorescence microscopy.[3,4] This fluorescence technique employs pulsed laser sources with femtosecond-wide pulses to excite fluorescent molecules. Previous MPM studies used high fluorophore concentrations (>500 μM), high laser power (>100 mW), optical clearing of tissues, or combinations of these factors to demonstrate improved imaging depth.[5–11] For example, a recent MPM study was able to image up to 1.6 mm deep in mouse brains after injection of Alexa 680.[5] However, this impressive imaging depth was reached with 5 mM dye concentration and >120 mW of

laser power incident on the sample. Similarly, another report achieved a 300 μm imaging depth in human tongue tissue without the use of exogenous labels,[8] albeit reaching a power of 160 mW at the surface. Although these studies highlight significant advances and the promise of MPM for deep-tissue imaging, the experimental conditions employed are not feasible for *in vivo* applications. Less damaging options are needed for minimally invasive preclinical and clinical use.

We and others have recently reported the use of NIR contrast agents in MPM, via excitation near 1550 nm and emission near 800 nm.[12–14] Owing to the low autofluorescence in the NIR, this all-NIR MPM approach (both excitation and emission are in the NIR wavelengths) has the potential to further enhance deep-tissue imaging. However, the absorption coefficient of water at 1550 nm is substantially higher than at the typical excitation wavelengths used in state-of-the-art MPM systems. Conceivably, biological materials that are composed of large amounts of water can attenuate the 1550-nm excitation intensity at greater depths, with an added risk of thermal damage to the tissue at high laser power. To establish the feasibility of all-NIR MPM for deep-tissue imaging, the penetration depth and tissue damage must be carefully evaluated.

Here, we report the comparison of three existing fluorescence microscopy systems: NIR single-photon confocal microscopy (NIR SPCM), state-of-the-art MPM, and all-NIR MPM. For clarity, we define the state-of-the-art MPM system that uses NIR excitation and acquires visible fluorescence images as NIR/VIS MPM and the all-NIR MPM system that employs both NIR excitation and NIR fluorescence imaging as NIR/NIR MPM. To perform the proposed comparison, we evaluated visible and NIR cyanine dyes in intact *ex vivo* mouse kidney after intravenous injection. Imaging depths of the different methods were compared, and the viability of cell and tissues exposed to NIR/NIR MPM was assessed for signs of photodamage in the target tissue.

2 Materials and Methods

2.1 Contrast Agents

Cy3 (PA23001, GE Healthcare, Piscataway, New Jersey) was used for systems imaging visible fluorescence. LS288 was synthesized as described previously[15] and used for systems imaging NIR fluorescence. For the cell imaging study, 3,3-diethylthiatricarbocyanine iodine (DTTCI; Sigma-Aldrich, St. Louis, Missouri) was used as an NIR fluorophore, and ethidium homodimer-1 (EthD-1; Life Technologies, Grand Island, New York) was used for the cell viability study. The structures and some optical properties of the dyes are provided in Table 1.

The hydrophilic dyes Cy3 and LS288 were used for the intact kidney tissue imaging, as they both clear through the kidneys. However, LS288 is not readily internalized by cells. We therefore used DTTCI for the cell studies, which has a similar chemical structure and comparable spectroscopic properties (Table 1) to LS288 but undergoes endocytosis.[16]

2.2 Ex Vivo Kidney Sample Preparation

Animal studies were performed in compliance with the Washington University School of Medicine (WUSM) Animal Studies Committee requirements for the humane care and use of laboratory animals in research. Ten-week-old male FVB/N mice were anesthetized with isoflurane (2% v/v in 100%

oxygen) via a precision vaporizer, and Cy3 or LS288 [100 μL of a 60 μM concentration in phosphate-buffered saline (PBS)] was administered intravenously via the lateral tail vein. Mice were euthanized 30 s after injection. Immediately after euthanasia, the kidneys were harvested intact and rinsed with PBS and subsequently imaged using the three microscopy methods.

2.3 Near-Infrared Single-Photon Confocal Microscopy

The NIR confocal microscope consists of a fiber-coupled laser diode (BDL-785-SMC, Becker-Hickl, Berlin, Germany); an upright confocal laser scanning fluorescence microscope (FV1000, Olympus, Center Valley, Pennsylvania); a 20×, 0.95-NA water-immersion objective lens (XLUMPLFLN 20XW, Olympus); a thermoelectrically cooled, red-enhanced photomultiplier tube (PMT) (PMC-100-20, Becker-Hickl); a time-correlated single-photon counting card (SPC-150, Becker-Hickl); and an inverter (A-PPI-D, Becker-Hickl).[16] At ~785 nm, the laser provides 60- to 80-ps-wide light pulses in TEM$_{00}$ mode with 80-MHz frequency. It is launched through a single-mode 1-m optical fiber (kineFLEX, Point Source, UK). The fiber provides an average laser power of 1.5 mW as its collimated output. The objective lens, which has a 2.0-mm working distance, is optimized for 0.17-mm-thick cover-glass, and provides ~65 to 75% transmittance at 700- to 900-nm wavelengths. The PMT operates in photon-counting mode from 300 to 900 nm. During image acquisition, a long-pass filter with cutoff of 800-nm wavelength was placed before the PMT to remove the residual excitation light. The captured images were saved in the host computer using the SPCImage software (Becker-Hickl). The spatial resolution of this system is 0.5 μm.[17] Far-red imaging was also performed using the Olympus FV1000 system using a 633-nm excitation continuous-wave laser embedded with this system and with emission captured in a passband of 645 to 745 nm. The spatial resolution of this system for XLUMPLFLN 20XW objective lens is 0.4 μm.[17]
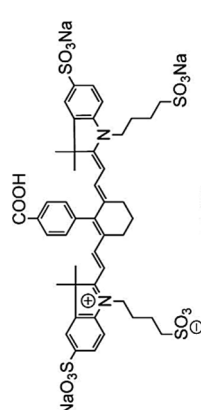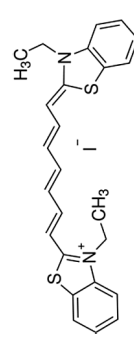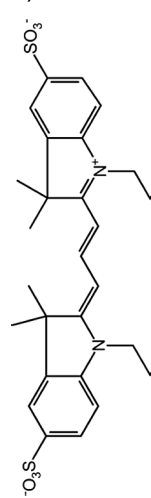
2.4 State-of-the-Art Multiphoton Microscopy

The NIR/VIS MPM system consists of an ultrafast Ti:Sapphire laser (Mai Tai BB, Spectra-Physics, Bozeman, Montana); an inverted multiphoton laser scanning fluorescence microscope (LSM-510-Meta-NLO, Zeiss, Germany); a 40×, 1.2-NA water-immersion objective lens (C-Apochromat, Zeiss); and a blue-enhanced multialkali PMT (R6357, Hamamatsu, Japan). At ~690 to 995 nm, the laser provides <80-fs-wide light pulses in TEM$_{00}$ mode with 80-MHz frequency. The average laser power is >250 mW in free space. The objective lens, which has a 0.28-mm working distance, is optimized for 0.17-mm-thick cover-glass and provides >80% transmittance at 400- to 800-nm wavelengths. The PMT operates in proportional mode at 185 to 900 nm, with peak sensitivity at 450 nm. Fluorescence emission was captured using long-pass and dichroic filter sets in the 560- to 650-nm window. The captured images were saved in the host computer using the LSM Image software (Zeiss). The spatial resolution of this system is 0.34 μm.[18]

2.5 All-Near-Infrared Multiphoton Microscopy

The NIR/NIR MPM system shown in Fig. 1 consists of a mode-locked fiber laser (Mercury 1550-200-150-INS, PolarOnyx, San

Table 1 Quantitative comparison between three microscopy methods in deep kidney tissue imaging.

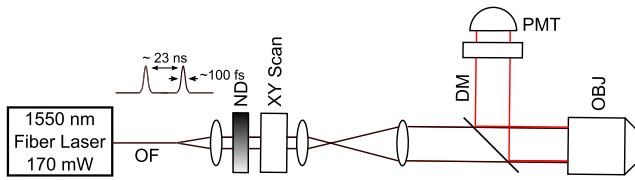| Microscopes	Confocal (single-photon confocal microscopy)		Multiphoton	
			Near-infrared (NIR)/NIR	NIR/visible (VIS)
Excitation wavelength (nm)	785	633	1575	900
Emission passband (nm)	>800	645 to 745	>700	560 to 650
Pixel integration time (μs)	7600	12.5	100	50
Detector module	PMC-100-20 (Becker-Hickl)	Integrated photomultiplier tube (FV1000, Olympus)	H7421-50 (Hamamatsu)	R6357 (Hamamatsu)
Laser dose (μJ/μm^2)	3.49 (Fig. 2), 0.06 (Fig. 3)	0.001	6.25	7.8
Objective lens	XLUMPLFLN 20XW (Olympus): 20×, 0.95-NA, water-immersion	XLUMPLFLN 20XW (Olympus): 20×, 0.95-NA, water-immersion	XLUMPLFLN 20XW (Olympus): 20×, 0.95-NA, water-immersion	C-Apochromat (Zeiss): 40×, 1.2-NA, water-immersion
Fluorescence decay constant in kidney (mm^{-1})	19.4 (Fig. 2)		6.26 (Fig. 2)	20.11 (Fig. 2)
Maximum depth penetrated in visualizing the renal structures (μm)	100 (Fig. 2)		533.4 (Fig. 2)	90 (Fig. 2)
Contrast-to-noise ratio computed down at 50 μm below the specimen surface corresponding to the equivalent average laser power and pixel integration time as used by the NIR/VIS MPM system	4.71 (Fig. 2)		10.22 (Fig. 2)	0.82 (Fig. 2)
Contrast agents		LS288[15]	DTTCI	Cy3
Structure				
Solvent		Phosphate-buffered saline (PBS)	PBS	PBS
Ex/Em (nm)		761/778	771/800	550/570
Extinction coefficient (M^{-1} cm^{-1})		122,000	87,000	150,000
Quantum yield		0.112	0.1	0.15
Brightness (M^{-1} cm^{-1})		13,664	8700	22,500

Fig. 1 Schematic of the near-infrared (NIR)/NIR multiphoton microscopy (MPM). OF, optical fiber; ND, neutral density filter; DM, dichroic mirror; OBJ, objective lens.

Jose, California); a galvanometric mirror pair (6215H, Cambridge Technology, Lexington, Massachusetts); a dichroic mirror (LP02-980RS, Semrock, Rochester, New York); the XLUMPLFLN 20XW objective lens; a thermoelectrically cooled, red-enhanced GaAs PMT and photon counting head (H7421-50, Hamamatsu); and a multifunction data acquisition card (PCI-6229, National Instruments, Austin, Texas).[12] The laser is centered at 1575 ± 20 nm with a frequency of 43.7 MHz, and it provides up to 200 mW of transform-limited (<150-fs-wide) pulses at the output of a 1-m single-mode fiber patch cord. The optical fiber was shortened (to ~0.75 m) to partially compensate for material dispersion in the system. The PMT operates in photon-counting mode at 380 to 890 nm, with peak sensitivity at 800 nm. A detailed discussion of this instrument, including data acquisition, point spread function measurements, and confirmation of the square-law relationship between the signal and incident power, is available elsewhere.[12] During image acquisition, a 3-mm-thick glass filter (RG9, Schott, Elmsford, New York) was used to remove the residual excitation light and capture fluorescence of >700 nm, with peak transmission at 780 nm. Custom-designed Labview software controls the image acquisition process. The spatial resolution of this system is 0.6 μm.[18]

2.6 Intralipid Phantom Imaging Using Multiphoton Microscopy

To determine the optimal wavelength needed for two-photon (2P) excitation of Cy3, fluorescence was measured from 2% intralipid diluted with 5 μM of the dye, which was placed in a glass-bottom dish (P35G-1.5-10-C, MatTek, Ashland, Massachusetts). This phantom was excited by the Ti:Sapphire laser (described in Sec. 2.4) at increasing wavelengths, ranging between 800 and 980 nm with 10-nm increments. During each wavelength measurement, the focal plane was adjusted to maximize fluorescence, and the 2P excitation wavelength of Cy3 obtained from the measured data corresponded to the maximum normalized average fluorescence. The highest fluorescence intensity was observed under an excitation wavelength of 900 nm, which was subsequently chosen for 2P excitation of Cy3. The peak excitation wavelength can vary under different experimental conditions, such as solvent and pH.[19]

2.7 Deep-Tissue Fluorescence Microscopy Imaging

For the upright microscope, the intact kidney samples were covered with a 0.17-mm-thick cover-glass. For the inverted microscope, the samples were placed in glass-bottom plates (MatTek), with 0.17-mm-thick coverslips. During imaging, the samples were excited with comparable total laser energies. NIR SPCM used 50 μW of laser power at 7.6 ms/pixel for 785-nm laser excitation and 27 μW of laser power at 12.5 μs/pixel for 633-nm laser excitation; NIR/VIS MPM used 30 mW of

laser power at 50 μs/pixel; and NIR/NIR MPM used 5.55 mW of laser power at 100 μs/pixel. A continuously variable neutral density (ND) filter (NDC-50C-2, Thorlabs, Newton, New Jersey) controlled the NIR/NIR MPM power. For the SPCM and NIR/VIS MPM systems, embedded ND filters controlled the power. For the NIR/NIR MPM, the incident power on the sample was computed analytically by considering absorption of water at 1550 nm. The effective incident power was computed using the equation

$$\varphi = \varphi_0 \exp(-\mu_a x), \quad (1)$$

where φ is the effective power of the light below a thick medium of width x, with an incident power of φ_0, and μ_a is the absorption coefficient of water at a given wavelength. Here, μ_a is 8.44 cm^{-1} at 1575 nm.[20] The 30-mW light emerging from the objective lens was reduced to 5.55 mW of incident power below the water-immersion media. This adjustment was not needed for the other two microscopes as water absorption is less prominent at 633, 785, and 900 nm.[21]

The minimal lateral spatial sampling intervals for NIR SPCM, NIR/VIS MPM, and NIR/NIR MPM were ~0.25, ~0.17, and 0.3 μm, respectively. These sampling intervals were computed following the Nyquist criterion. Image stacks were captured with a field of view (FOV) of 42×42 μm^2 or 318×318 μm^2 with 2- to 20-μm steps during NIR SPCM imaging, 225×225 μm^2 with 1-μm steps during NIR/VIS MPM imaging, and 172×172 μm^2 with 25.4-μm steps during NIR/NIR MPM imaging. To capture the stacks along the axial direction, the NIR SPCM and NIR/VIS MPM systems used translation stages with embedded closed-loop motorized actuators, and the NIR/NIR MPM used a manual translation stage (MT3, Thorlabs).

2.8 Quantification of Fluorescence and Contrast-to-Noise Ratio

To quantitatively compare depth penetration performances of the three microscopy methods, we computed the fluorescence attenuation in tissue and computed the contrast-to-noise ratio (CNR) to identify specific structures.

The average fluorescence signal versus depth was fit with a simple single-exponential decay.

$$y = y_0 \exp(-\alpha z). \quad (2)$$

Here y_0 and y are the average fluorescence at the plane of focus and the fluorescence after transmission for a distance z through the heterogeneous tissue, respectively. α represents the attenuation of the fluorescence signal, for the respective microscopy method. Although more complex models such as those based on a diffusion approximation of the radiative transfer equation[22] may represent light propagation through tissue more accurately, Eq. (2) was used because of its inherent simplicity and sufficient power to provide a first-order estimate for comparing the imaging depth of the three microscopy modalities.

To identify renal tubules in the tissue images, the CNR was computed for every image at each depth location. The image CNR in a renal tubule is

$$CNR = \frac{\hat{m}_r - \hat{m}_b}{\sqrt{\hat{m}_r} + \sqrt{\hat{m}_b}}, \quad (3)$$

where $\hat{m}$ denotes the fluorescence mean, and the subscripts r and b denote a region of interest (i.e., renal tubule) and its adjacent background, respectively. Note that the decay constant α is independent of the laser power, pixel integration time, and fluorescence concentration used in imaging, while CNR depends on these factors. Given that large samples are used to compute $\hat{m}$ in Eq. (3) and PMTs work under the shot noise regime, CNR scales as the square root of pixel integration time. Under the same assumption, this metric scales with the square root of the average laser power for single-photon imaging, and directly with such average power for 2P imaging. These properties describing the relationship of CNR with pixel integration time and with average laser power were employed to normalize the CNR attenuations obtained from different microscopy methods to compare their depth penetration performances.

2.9 Cell Viability Study for All-Near-Infrared Multiphoton Microscopy

Mouse leukemic monocyte macrophage (Raw264.7; Tissue Culture Support Center, WUSM, St. Louis, Missouri) cells were grown uniformly in a glass-bottom culture dish (MatTek) of 10-mm well diameter. Cells were cultured in Dulbecco's modified Eagle medium (Invitrogen, Grand Island, New York) supplemented with 10% fetal bovine serum and 1% penicillin–streptomycin 100× (Invitrogen), and maintained at 37°C in a humidified atmosphere of 5% CO_2 before conducting the NIR/NIR MPM imaging. When ∼80% confluency level was reached, the cells were treated with 5 μM DTTCI for 30 min, and 30 different regions of the glass-bottom dish containing the cells were then imaged using the NIR/NIR MPM system. Each region in FOV of 0.628×0.628 mm, constituting 256×256 pixels, was exposed to the 1550-nm laser for a 1-ms/pixel integration time, using 5.55 mW of laser power. These settings allowed exposure of ∼15% area of the glass-bottom to the 1550-nm laser by using a similar setup as employed for conducting the NIR/NIR MPM depth penetration study.

DTTCI-treated and untreated Raw264.7 cells that were not exposed to the 1550-nm laser served as negative controls for the study. For each of these control sets, one fraction of cells was maintained at 37°C in a humidified atmosphere of 5% CO_2. The rest were kept at room temperature during imaging of the DTTCI-treated cells using NIR/NIR MPM. As positive controls, Raw264.7 cells were treated with ethanol for 30 min. These cells were kept at 37°C in a humidified atmosphere of 5% CO_2 and were not exposed to the 1550-nm laser.

Upon completion of the NIR/NIR MPM imaging, the cells were treated with EthD-1 for 45 min to differentiate live and dead cells. Differential interference contrast (DIC) and fluorescence images were obtained using the confocal microscope described in Sec. 2.3, with 11.2 μW of 543-nm laser excitation, 12.5-μs/pixel integration time, and fluorescence acquisition at 555 to 655 nm. During this process, 10 separate very slightly overlapped sets of DIC images and fluorescence images of cells were captured from each glass-bottom dish. Each image had 512×512 pixels collected over an FOV of 3.18×3.18 mm, and collectively the 10 images encompassed the entire culture dish. In each captured image, the total number of cells and total number of dead cells were counted from the DIC and fluorescence images, respectively, using the ImageJ *Cell Counter* plugin. The fraction of dead cells was computed from each image, and the resulting fractions were averaged.

2.10 Tissue Viability Study for All-Near-Infrared Multiphoton Microscopy

To further determine the potential for tissue photodamage, intact kidneys were harvested from two FVB/N mice injected with LS288. One of these kidneys was imaged using the NIR/NIR MPM system in 10 adjacent regions. Each region with a scan volume of $0.628 \times 0.628 \times 0.406$ mm, comprising $256 \times 256 \times 16$ pixels, was exposed to the 1550-nm laser for 1-ms/pixel integration time. The distance between focal planes was 25.4 μm. The incident laser power on the sample was 5.55 mW. The total exposed area was ∼6.28×6.28 mm.

The second and third kidney samples were used as negative controls. One was kept in the same ambient environment as the test sample during NIR/NIR MPM imaging, while the other was immediately fixed in 4% paraformaldehyde at 4°C as described below. As a positive control, the fourth kidney sample was briefly damaged using a cauterizing pen (AA01, Bovie Medical, Clearwater, Florida) at 10 different locations up to 1 mm depth.

Kidney samples were fixed overnight in 4% paraformaldehyde at 4°C, then in alcohol gradients up through 70% concentration, and finally embedded in paraffin. Tissue sections of 5 μm thickness from the top 200 μm were cut using a microtome (Cryocut 1800, Leica Biosystems, Buffalo Grove, Illinois) and stained with hematoxylin and eosin (H&E). The resulting slices were imaged using a microscope (BX51, Olympus) equipped with 20×, 0.5-NA air objective lens (UPLFLN, Olympus); 100×, 1.25-NA oil objective lens (Plan, Nikon, Melville, New York); and a color camera (DP71, Olympus). The images covered 1360×1024 pixels, and the FOV on the sample was 186×140 μm for the 100× objective lens and 930×700 μm for the 20× objective lens.

3 Results and Discussion

3.1 Cyanine Dyes with Structural Homology Provide Imaging Contrast in the Visible and Near-Infrared Wavelengths for Single- and Two-Photon Microscopy

The advent of *in vivo* imaging of molecular processes with NIR fluorescent probes has led to the development of NIR SPCM[2] and most recently an NIR/NIR MPM.[6,12,14] A vexing question addressed in this study is the relationship between the different NIR excitation and emission wavelengths and the imaging depth in tissue. To assess the enhancement of imaging depth with the two different all-NIR microscopic methods relative to the traditional MPM with detection in the visible wavelengths, we used LS288, DTTCI, and Cy3 dyes. Cy3 is widely used for NIR/NIR MPM studies,[23] and thus NIR/VIS MPM depth profiling study using Cy3 will serve as a reference for the newer all-NIR microscopy techniques. LS288 is a highly hydrophilic molecule that is excreted by the kidneys.[24] This clearance pathway allowed significant uptake of both LS288 and Cy3 in the kidneys, which were harvested for the microscopy studies. However, LS288 does not readily internalize in cells and could not be used for the NIR microscopy in cells. To overcome this limitation, we used DTTCI for the cell studies, which readily internalizes in cells.[16] Both LS288 and DTTCI have similar chemical structures and spectral properties (Table 1). This overall process thus allowed for comparative evaluation of three different microscopy modalities. The homology of the dye structures and similarity in their optical properties also allowed

similar response in tissue microscopy, thereby minimizing variability from disparate spectral properties of different dyes.

3.2 Near-Infrared Confocal and State-of-the-Art Multiphoton Microscopy Demonstrate Similar Imaging Depth in Tissues

Using NIR SPCM, based on fluorescence alone, we visualized LS288 within renal structures, including the renal tubules in the kidney cortex,[25] down to ~100 μm below the specimen surface (Fig. 2). In two other experiments, using the 633- or the 785-nm laser of the NIR SPCM, we were able to image down to ~60 μm below the respective specimen surfaces for intact kidney samples from two different mice (Fig. 3). Using the NIR/VIS MPM system at this wavelength, we visualized similar renal structures down to ~90 μm below the specimen surface (Fig. 2). This demonstrates that NIR SPCM is comparable to NIR/VIS MPM for interrogating molecular events in deep tissues. However, the spatial resolution is higher in the shorter (visible) than the longer (NIR) wavelengths. Therefore, a tradeoff between imaging depth and resolution as well as the biological question must be considered to determine the best method for any study. This finding also provides a unique opportunity for multiplexing information. For example, an 800-nm laser can be used to excite an NIR dye and a visible dye by single-photon and 2P excitation, respectively, providing an opportunity to interrogate two or more molecular events at similar depths.

3.3 All-Near-Infrared Multiphoton Microscopy Has Higher Imaging Depth Than Both NIR Confocal Microscopy and State-of-the-Art MPM

Using the NIR/NIR MPM system to image fresh-frozen intact kidney samples from different mice containing LS288, the fluorescence contrast was detected from the surface down to >500 μm (Figs. 2 and 3). Renal tubules were visualized, similar to those seen with the other two microscopy techniques. The results show that the NIR/NIR MPM system could image more than fivefold deeper than the other two microscopy techniques under similar imaging conditions. This result reflects the
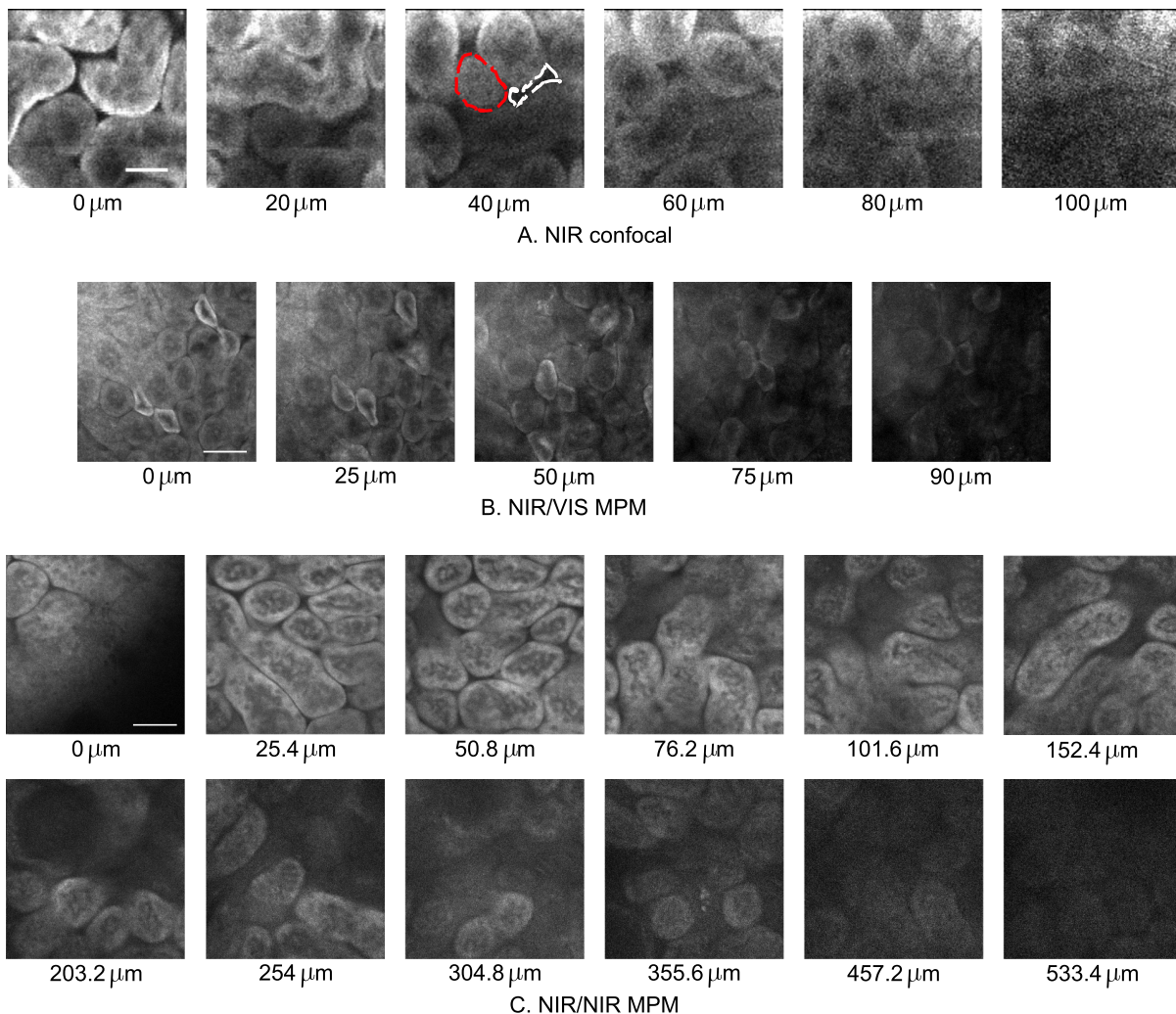

Fig. 2 NIR confocal microscopy image stack (scale bar is 9 μm) (a). NIR/visible (VIS) MPM image stack (scale bar is 45 μm) (b). NIR/NIR MPM image stack (scale bar is 34 μm) (c) of mouse kidney *ex vivo*. Mouse kidneys were harvested after intravenous injection of NIR dye LS288 [(a) and (c)] and of visible dye Cy3 (b). The structure of renal tubules in the kidney cortex can be visualized down to ~100 μm below the specimen surface for NIR confocal microscopy (a), down to ~90 μm below the specimen surface for NIR/VIS MPM (b), and down to >500 μm below the specimen surface for NIR/NIR MPM (c). Dashed red lines and white lines in one of the images in (a) depict examples of a renal tubule region r and its adjacent background region b.

10 μm   60 μm
NIR confocal (additional example 1)

14 μm   60 μm
NIR confocal (additional example 2)

25.4 μm   457.2 μm
NIR/NIR MPM (additional example 1)

101.6 μm   508 μm
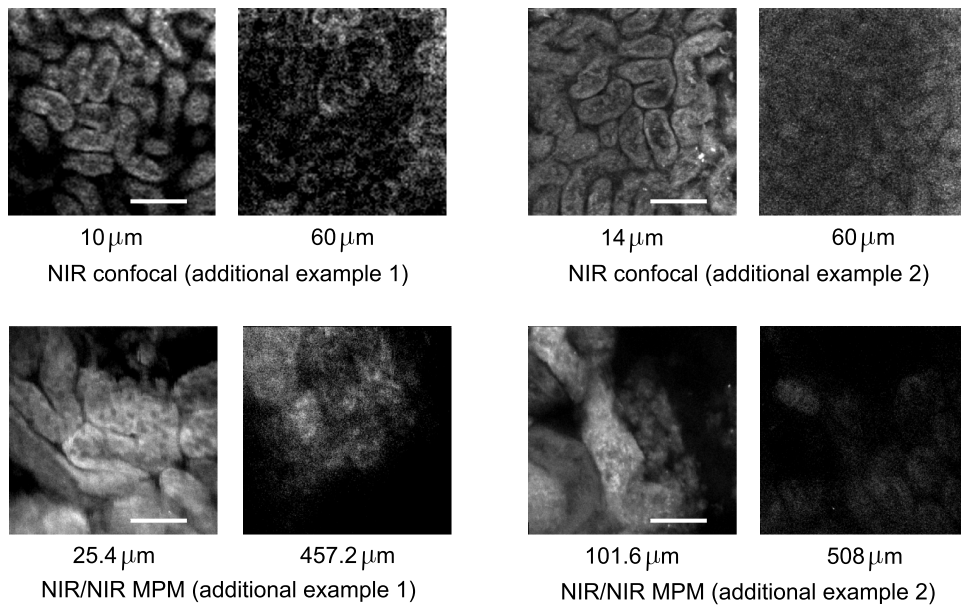NIR/NIR MPM (additional example 2)

Fig. 3 Additional depth penetration imaging results using mice kidneys *ex vivo*, harvested after intravenous injection of NIR dye LS288. Kidneys from different animals were imaged using NIR confocal microscopy method and NIR/NIR MPM method. Similar tubular structures as shown in Fig. 2 can be visualized. For the second example using NIR confocal microscopy depicted herein, we used laser excitation from a 633-nm laser with emission captured in 645-to-745-nm window. Microscopic structures were visualized down to ~60 μm in examples using the NIR confocal system and down to ~508 μm in examples using the NIR/NIR MPM system. Scale bars are 91 and 49 μm for the confocal and the MPM methods, respectively.

combined benefits of lower scattering and absorption of the NIR light used for both dye excitation and emission, as well as the selective focal plane illumination of the 2P imaging mechanism.

Unlike the images obtained with the NIR confocal microscopy and NIR/VIS MPM, the detected fluorescence intensity of the NIR/NIR MPM images decreased more slowly with tissue depth (Fig. 4). For the result shown in Fig. 2, fluorescence signal measurements along the depth from several locations of renal tubular structures were averaged, and the fluorescence signal decay constants in the kidney were computed using a single-exponential fit [Eq. (2)]. Corresponding values of 19.4, 20.11, and 6.26 mm^{-1} were determined for the NIR SPCM,

NIR/VIS MPM, and NIR/NIR MPM, respectively. The comparable signal attenuation in the kidney using the NIR confocal microscopy and NIR/VIS MPM techniques indicates that these systems penetrate similarly in deep tissues during fluorescence imaging. This result also confirms that the NIR/NIR MPM system offers more than threefold lower attenuation of fluorescence in deep kidney tissue.

To compare the penetration depths of the three microscopes, CNR attenuations were normalized corresponding to the equivalent average laser power and pixel integration time as used by the NIR/VIS MPM system for imaging. Five to 10 renal tubules and their adjacent background regions from each image were manually selected to compute CNR attenuations based on
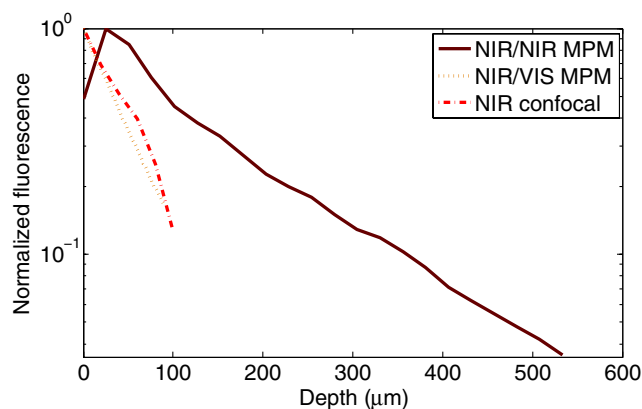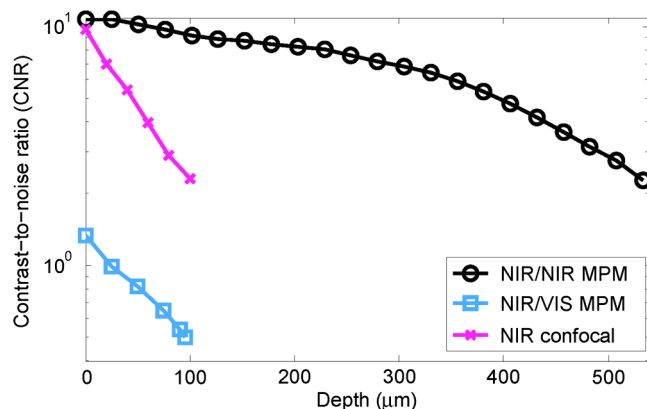

Fig. 4 Comparison of normalized foreground fluorescence detected at given depths in deep tissues using the three microscopy modalities. Fluorescence measurements along the depth from several locations of renal tubular structures were averaged for the images in Fig. 2. The NIR confocal microscope and NIR/VIS MPM perform similarly in penetrating deep tissues, while the new NIR/NIR MPM system offers more than threefold lower signal attenuation in deep kidney tissues.

Fig. 5 Normalized contrast-to-noise ratio (CNR) in identifying renal tubules in imaging deep tissues using three microscopy modalities. Measured data demonstrate that the NIR confocal microscope performs better than the NIR/VIS MPM system. The NIR/NIR MPM system performs significantly better than the others in identifying renal tubules in deep kidney tissues.

Eq. (3) for the result shown in Fig. 2. Representative examples of one such renal tubule r and its adjacent background b are shown in Fig. 2(a). Resulting normalized CNRs were compared to identify renal tubules in captured images (Fig. 5). In the kidney, the CNR of the NIR SPCM system is higher than that of the NIR/VIS MPM system up to the maximum depth examined in this study. The NIR/NIR MPM system offers the highest CNR in the kidney. Table 1 summarizes the quantitative data described in this section. From previous reports, it is expected that an increase in excitation power would shift CNR attenuation curves to the right for all systems.[6] Increments of excitation power also increase the potential for tissue damage.

Although the dye used for NIR/VIS MPM (Cy3) is brighter than that used for NIR/NIR MPM (LS288), the latter system achieves deeper imaging. We further note that the brightnesses of LS288 and of Cy3 reported in Table 1 are their single-photon brightnesses, and one needs to consider their 2P brightness values for a more quantitative comparison. Nonetheless we selected these dyes for our study as Cy3 is known for its high 2P absorption cross-section [19] and is widely used for NIR/VIS MPM studies,[23] and LS288 is structurally homologous to Cy3. Ideally, this study should be conducted with dyes possessing similar single-photon brightness values and two-photon absorption cross-sections if they become available.
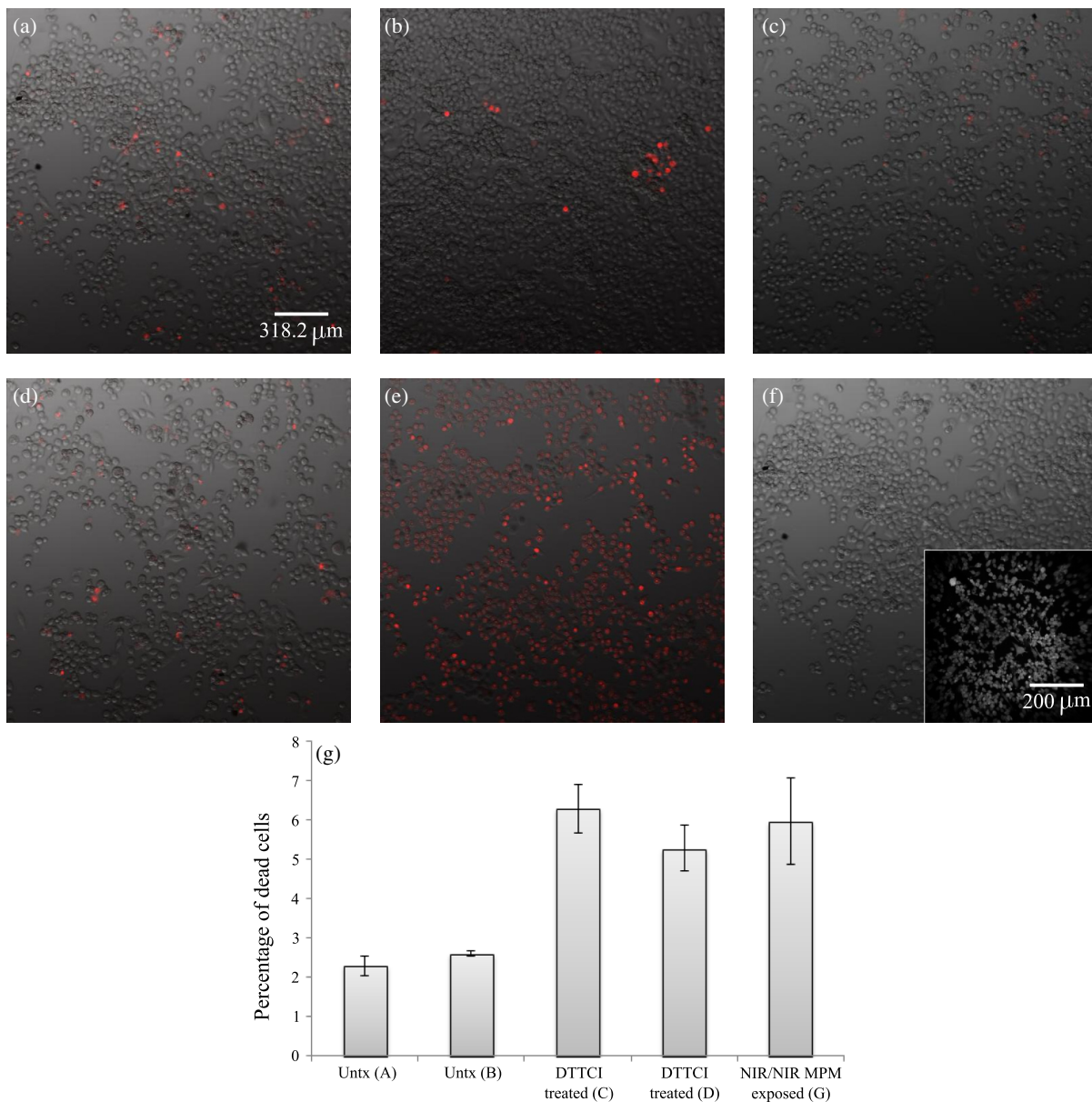

Fig. 6 Results of cell viability due to laser exposure. Red fluorescence from the cell viability indicator ethidium homodimer-1 (EthD-1) is overlaid on differential interference contrast (DIC) images of cells in culture. (a) and (b) are representative images of negative control cells that were neither treated with 3,3-diethylthiatricarbocyanine iodine (DTTCI) nor exposed to the 1550-nm laser. (c) and (d) are representative images of cells treated with DTTCI but not exposed to the laser. (e) is a representative image of positive control cells, treated with ethanol. (f) is a representative image of cells treated with DTTCI and later exposed to the NIR/NIR MPM system. The inset shows a representative 2P image of such cells. (g) shows the percentage of dead cells in the respective populations whose samples are shown in (a) to (d) and (f). The study finds that DTTCI slightly reduces cell viability relative to negative controls. In contrast, exposure to the laser under the NIR/NIR MPM system does not result in any additional reduction in cell viability.

3.4 All-Near-Infrared Multiphoton Microscopy System Does Not Photodamage Cells and Tissues During Imaging

Water absorption is >100 times higher at 1550 nm than the tissue transparent window of 700 to 900 nm.[20,21,26] It is therefore important to assess whether the new NIR/NIR MPM system penetrates deeper than the other two systems at the cost of damaging the target tissue. With femtosecond laser exposure, the maximum temperature rise, T_{max}, in a sample undergoing 2P imaging is given by[27]

$$T_{max} = \frac{E\mu_a f_{rep}}{4\pi k_t} \ln\left(1 + \frac{2t_{exp}}{\tau_c}\right) + \frac{E\mu_a}{2\pi k_t \tau_c}, \qquad (4)$$

where μ_a is the absorption coefficient, f_{rep} is the laser repetition rate, k_t is tissue thermal conductivity, with a typical value of 0.6 W/K/m,[27] t_{exp} is the exposure time at the spot where laser beam is exposed to the sample, τ_c is the thermal diffusion time of water in tissue, which is ~70 ns,[27] and E is the laser energy per pulse. Because there is no reported value for the absorption coefficient of kidney tissue at 1575 nm, we used the coefficient ($\mu_a = 1.1$ mm^{-1}) reported for liver tissue at this wavelength.[28] The temperature increase was estimated to be 7°C during the NIR/NIR MPM imaging described in Sec. 2.7. Assuming the sample temperature was 37°C, the resulting increase would be 44°C, which is well below the threshold for denaturation of structural proteins (~60°C) or vaporization of water (~100°C).[29] These are good indicators of a biocompatible imaging condition.

Cells are assumed to be predominantly aqueous, and thus we estimate the absorption coefficient of the cells with that of water ($\mu_a = 8.44$ cm^{-1}).[20] Thus, the estimated maximum temperature rise of live Raw264.7 cells was 6.8°C, corresponding to T_{max} of 43.8°C, during imaging using the NIR/NIR MPM system (see Sec. 2.9). No significant difference was found in the number of dead cells between the DTTCI-treated cells that were either exposed or not exposed to the NIR/NIR MPM laser. Expectedly, the positive control cells were all dead.

Figure 6 shows representative images from the cell viability assay for control and laser-exposed samples. Red fluorescence from the cell viability indicator EthD-1 is superimposed on DIC images of the cell population in the FOV. For the 2P imaged sample, Fig. 6(f) shows in the inset a representative gray-scale image of cells imaged using the NIR/NIR MPM system. Figure 6(g) presents the fraction of dead cells in the negative control samples and the NIR/NIR MPM imaged samples. DTTCI is shown to slightly reduce cell viability relative to negative controls. In contrast, the NIR/NIR MPM system does not damage the cells any further, resulting in a comparable fraction of cell death without laser exposure. In this study, ~15% cells were exposed to the 1550-nm laser under similar conditions used in the depth penetration study. Therefore, in the event of cell damage caused by this system, a statistically significant percentage difference between the number of dead cells in the NIR/NIR MPM imaged sample and the cells that were only treated with DTTCI was expected. Figure 6(g) does not show such a difference, validating the compatibility of the imaging system with biological samples.

We have imaged cells with the NIR/NIR MPM system and subsequently imaged the same cells with a confocal microscope after staining with EthD-1. Both DTTCI-treated and untreated cells were imaged, as shown in Fig. 7. To ensure that the exact same area was imaged, DTTCI-soaked tissue paper was placed underneath the MatTek dishes to indicate the 1550-nm laser exposure regions. Locations of tissue paper corners [Figs. 7(a), 7(c), 7(e), and 7(g)] for both experiments were identified and served as fiducial markers using the NIR/NIR MPM system and the DIC mode of the confocal system. Figures 7(b) and 7(f) represent fluorescence images of 1550-nm laser-exposed regions. Figures 7(c) and 7(g) represent DIC images of the 1550-nm laser-exposed regions (shown using white circles) and their surroundings. Figures 7(d) and 7(h) show corresponding red fluorescence from the cell viability indicator EthD-1, with exposed regions using red circles. No significant difference in cell death between the 1550-nm exposed region and the other region was observed in both cases. Moreover, the 1550-nm exposed cells show well attachment with the
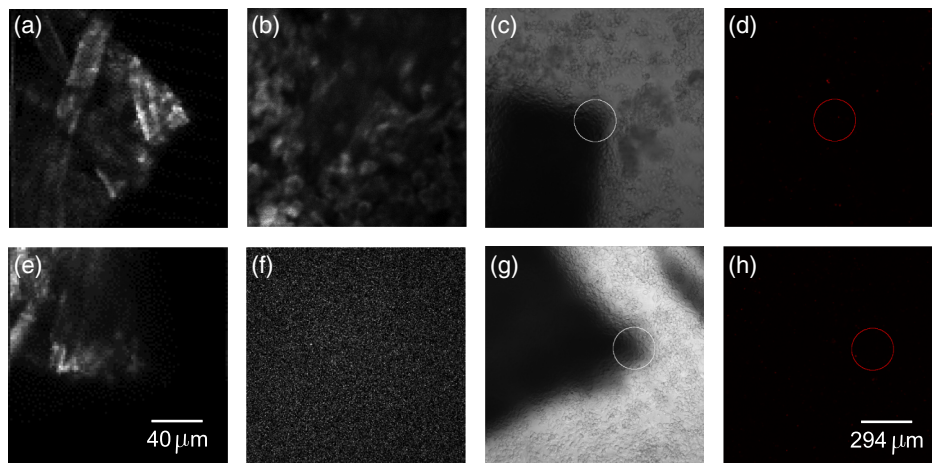

Fig. 7 Additional results of cell viability due to laser exposure. Cells were either treated [(a) to (d)] or untreated [(e) to (h)] with DTTCI on MatTek dishes. They were exposed to the NIR/NIR MPM system. DTTCI-stained tissue paper was placed underneath the MatTek dishes to mark the 1550-nm laser exposure regions. (a) and (e) represent NIR/NIR MPM images of such marks. (b) and (f) represent corresponding regions on the dishes exposed to the 1550-nm laser. (c) and (g) represent DIC images of the exposed regions (shown using white circles) and their surroundings. (d) and (h) show corresponding red fluorescence from the cell viability indicator EthD-1, with exposed regions using red circles. No significant difference in cell death between the 1550-nm exposed region and unexposed regions was observed in both cases.

cell culture dish, as demonstrated in the DIC images, suggesting good cell health. Similar results were obtained in three duplicated experiments. The 1550-nm laser-unexposed regions here show less cell death than the untreated cell experiment presented in Fig. 6.

Further, histological studies confirmed that the NIR/NIR MPM imaging does not damage tissues. Using Eq. (4), the estimated maximum temperature rise of the kidney sample during NIR/NIR MPM imaging was 8.8°C, resulting in a T_{max} of 45.8° C. Neither the negative nor positive control samples were exposed to the NIR/NIR MPM system, but the latter was damaged using a cauterizing pen (see Sec. 2.10). Figure 8 shows representative H&E images of tissue sections obtained from these four samples (see Sec. 2.10 for method description). There is no noticeable difference between the tissue morphologies of the 2P imaged tissue and the negative control tissue, as confirmed by a board-certified pathologist. In contrast, the positive control tissue section shows a significant difference in morphology. Thermal damage due to cauterization caused necrosis of the tissue, indicated by a breakdown of tissue morphology and collapsed nuclei near the damaged location.

These theoretical, experimental, and pathological assessments support the conclusion that the NIR/NIR MPM system's dramatic increase in depth resolution was not achieved at the cost of damaging the underlying tissues of interest.

3.5 NIR/NIR MPM Achieves Imaging Depth > 533 μm in the Kidney

The NIR/NIR MPM imaging results demonstrate that, in the same tissues, this technique can image more than five times deeper than the confocal microscopy and NIR/VIS MPM systems. This performance comparison, however, is relative. Namely, the CNR was improved about twofold by a collection of factors, including imaging 256×256 pixels at 533.4 μm depth in kidney and using 1-ms/pixel laser excitation while keeping other imaging parameters unchanged, as described in Sec. 2.7 (Fig. 9). The CNR in identifying renal tubules in this image is 1.5 ± 0.38, for 5.55-mW power and 1-ms/pixel integration time of the 1550-nm laser. In contrast, the same
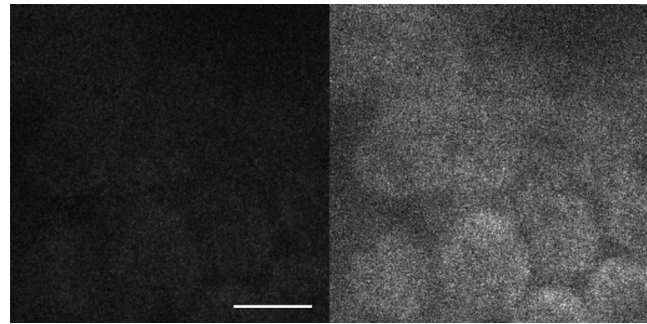

Fig. 9 Side-by-side comparison of images captured using the NIR/NIR MPM system, at 533.4 μm depth in an *ex vivo* intact mouse kidney. This organ was harvested after intravenous injection of NIR dye LS288. Scale-bar length is 34 μm. The images were originally captured in 575×575 pixels with 0.1-ms pixel integration time and in 256×256 pixels with 1-ms pixel integration time, respectively. The latter image offers almost twofold better CNR than the former. In both cases, the associated tissues did not suffer any damage.

FOV using 5.55-mW power of 1550-nm laser excitation with 0.1 ms/pixel (Fig. 2) depicted relatively unclear features of the same renal structures, with a computed CNR of 0.59 ± 0.33. This difference suggests that the absolute depth penetration limit of the NIR/NIR MPM system could be improved by higher laser energy along the *z*-direction, as employed in a recent work using three-photon microscopy.[6] Importantly, penetration depth >533.4 μm can be achieved for relatively more transparent tissues than the kidney, such as brain under the same experimental conditions. When tissue viability is not critical, researchers can image deeper than 533.4 μm with the NIR/NIR MPM system, as long as the high laser dose does not damage structural integrity of the underlying tissues.

4 Conclusion

Using cyanine-based contrast agents, we compared the *ex vivo* depth resolutions of three fluorescence microscopy modalities: single-photon NIR confocal, state-of-the-art MPM, and all-NIR
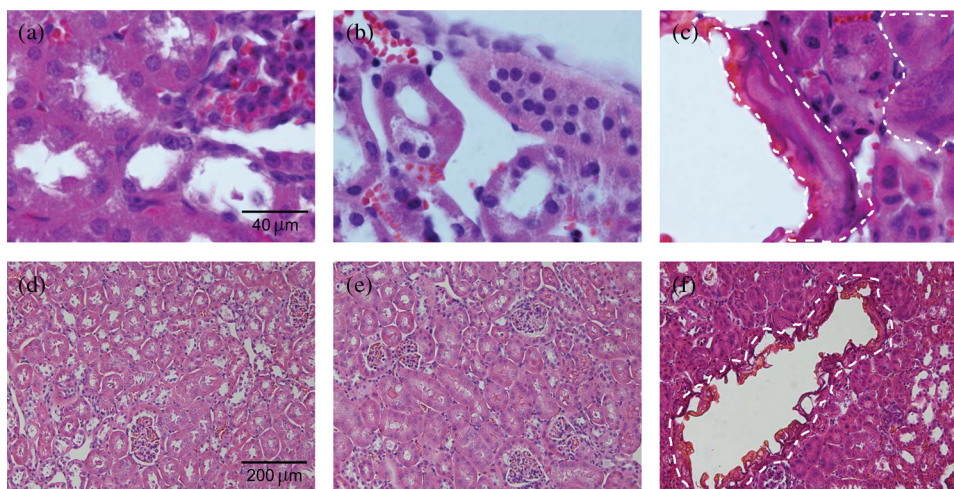

Fig. 8 Representative color images of histological sections of mouse kidney tissues: (a) and (d) exposed to 1550-nm light for imaging with the NIR/NIR MPM system, (b) and (e) untreated, and (c) and (f) thermally damaged by brief contact with cauterizing pen. There was no detectable difference between the NIR/NIR MPM imaged sample and the nonimaged controls, but thermal damage from cauterization is easily apparent. Dashed white lines in (c) and (f) highlight damaged regions. Thermal damage due to cauterization caused necrosis of the tissue, indicated by a breakdown of tissue morphology and collapsed nuclei near the damaged location. (a) to (c) represent 100× images and (d) to (f) represent 20× images.

MPM systems. For all three techniques, comparable experimental protocols were followed, including measurement at equal time points following intravenous injection and use of similar laser dose. The results suggest that (1) through the use of NIR dyes, single-photon NIR confocal microscopy performs similarly to the NIR/VIS MPM systems using visible dyes and (2) the NIR/NIR MPM penetrates about five times deeper in kidney tissues than the other systems used in this study. The depth penetration limit using the NIR/VIS MPM system agrees well with the literature.[30] Furthermore, cytological and histological studies indicate that under normal imaging conditions, NIR/NIR MPM does not damage the sample, in spite of the high water absorption at the excitation wavelength.

In future work, we will use contrast agents that have similar single-photon and 2P brightness and absorption cross-sections.[13] We will also investigate depth penetration performances of the NIR/NIR MPM system in kidneys of different preclinical disease mouse models. The current study provides important guidance on the imaging depth capabilities of different microscopy techniques based on NIR-based excitation at different wavelengths. A conceivable benefit of the all-NIR microscopy is the potential to multiplex imaging information in a tissue region with traditional visible light microscopy.

Acknowledgments

References

1. K. W. Dunn and T. A. Sutton, "Functional studies in living animals using multiphoton microscopy," *ILAR J.* **49**(1), 66–77 (2008).
2. S. Achilefu et al., "Synergistic effects of light-emitting probes and peptides for targeting and monitoring integrin expression," *Proc. Natl. Acad. Sci. U.S.A.* **102**(22), 7976–7981 (2005).
3. W. Denk et al., "Two-photon laser scanning fluorescence microscopy," *Science* **248**(4951), 73–76 (1990).
4. W. R. Zipfel et al., "Nonlinear magic: multiphoton microscopy in the biosciences," *Nat. Biotechnol.* **21**(11), 1369–1377 (2003).
5. D. Kobat et al., "In vivo two-photon microscopy to 1.6-mm depth in mouse cortex," *J. Biomed. Opt.* **16**(10), 106014 (2011).
6. N. G. Horton et al., "In vivo three-photon microscopy of subcortical structures within an intact mouse brain," *Nat. Photonics* **7**(3), 205–209 (2013).
7. F. Helmchen and W. Denk, "Deep tissue two-photon microscopy," *Nat. Methods* **2**(12), 932–940 (2005).
8. N. J. Durr et al., "Maximum imaging depth of two-photon autofluorescence microscopy in epithelial tissues," *J. Biomed. Opt.* **16**(2), 026008 (2011).
9. H. Hama et al., "Scale: a chemical approach for fluorescence imaging and reconstruction of transparent mouse brain," *Nat. Neurosci.* **14**(11), 1481–1488 (2011).
10. W. Jiang et al., "Assessing near-infrared quantum dots for deep tissue, organ, and animal imaging applications," *J. Lab. Autom.* **13**(1), 6–12 (2008).
11. P. Theer et al., "Two-photon imaging to a depth of 1000 micron in living brains by use of a Ti:Al₂O₃ regenerative amplifier," *Opt. Lett.* **28**(12), 1022–1024 (2003).
12. S. Yazdanfar et al., "Multiphoton microscopy with near infrared contrast agents," *J. Biomed. Opt.* **15**(3), 030505 (2010).
13. M. Y. Berezin et al., "Two-photon optical properties of near-infrared dyes at 1.55 mum excitation," *J. Phys. Chem. B* **115**(39), 11530–11535 (2011).
14. K. Murari et al., "Compensation-free, all-fiber-optic, two-photon endomicroscopy at 1.55 mum," *Opt. Lett.* **36**(7), 1299–1301 (2011).
15. H. Lee et al., "Heptamethine cyanine dyes with a robust C-C bond at the central position of the chromophore," *J. Org. Chem.* **71**(20), 7862–7865 (2006).
16. R. Nothdurft et al., "Fluorescence lifetime imaging microscopy using near-infrared contrast agents," *J. Microsc.* **247**(2), 202–207 (2012).
17. J. Pawley, *Handbook of Biological Confocal Microscopy*, Springer, New York (2006).
18. M. Gu, "Image formation in multiphoton fluorescence microscopy," in *Handbook of Biomedical Nonlinear Optical Microscopy*, B. R. Masters and P. T. C. So, Eds., pp. 266–282, Oxford University Press, New York (2008).
19. M. A. Albota et al., "Two-photon fluorescence excitation cross sections of biomolecular probes from 690 to 960 nm," *Appl. Opt.* **37**(31), 7352–7356 (1998).
20. D. M. Wieliczka et al., "Wedge shaped cell for highly absorbent liquids: infrared optical constants of water," *Appl. Opt.* **28**(9), 1714–1719 (1989).
21. K. F. Palmer and D. Williams, "Optical-properties of water in near-infrared," *J. Opt. Soc. Am.* **64**(8), 1107–1110 (1974).
22. M. S. Patterson et al., "Time resolved reflectance and transmittance for the non-invasive measurement of tissue optical properties," *Appl. Opt.* **28**(12), 2331–2336 (1989).
23. F. Bestvater et al., "Two-photon fluorescence absorption and emission spectra of dyes relevant for cell imaging," *J. Microsc.* **208**(2), 108–115 (2002).
24. R. J. Goiffon et al., "Dynamic noninvasive monitoring of renal function in vivo by fluorescence lifetime imaging," *J. Biomed. Opt.* **14**(2), 020501 (2009).
25. A. Vander, *Renal Physiology*, McGraw-Hill Professional Publishing, New York (1994).
26. G. M. Hale and M. R. Querry, "Optical constants of water in the 200-nm to 200-microm wavelength region," *Appl. Opt.* **12**(3), 555–563 (1973).
27. B. R. Masters et al., "Mitigating thermal mechanical damage potential during two-photon dermal imaging," *J. Biomed. Opt.* **9**(6), 1265–1270 (2004).
28. P. Parsa et al., "Optical properties of rat liver between 350 and 2200 nm," *Appl. Opt.* **28**(12), 2325–2330 (1989).
29. R. R. Anderson and J. A. Parrish, "Selective photothermolysis: precise microsurgery by selective absorption of pulsed radiation," *Science* **220**(4596), 524–527 (1983).
30. H. Bao et al., "Fast handheld two-photon fluorescence microendoscope with a 475 microm x 475 μm field of view for in vivo imaging," *Opt. Lett.* **33**(12), 1333–1335 (2008).